

A cytochrome P450 CYP87A4 imparts sterol side-chain cleavage in digoxin biosynthesis

Received: 25 January 2023

Accepted: 20 June 2023

Published online: 08 July 2023

Emily Carroll^{1,2}, Baradwaj Ravi Gopal^{1,2}, Indu Raghavan¹,
Minakshi Mukherjee¹ & Zhen Q. Wang¹✉

Digoxin extracted from the foxglove plant is a widely prescribed natural product for treating heart failure. It is listed as an essential medicine by the World Health Organization. However, how the foxglove plant synthesizes digoxin is mostly unknown, especially the cytochrome P450 sterol side chain cleaving enzyme (P450_{scc}), which catalyzes the first and rate-limiting step. Here we identify the long-specified foxglove P450_{scc} through differential transcriptomic analysis. This enzyme converts cholesterol and campesterol to pregnenolone, suggesting that digoxin biosynthesis starts from both sterols, unlike previously reported. Phylogenetic analysis indicates that this enzyme arises from a duplicated cytochrome P450 *CYP87A* gene and is distinct from the well-characterized mammalian P450_{scc}. Protein structural analysis reveals two amino acids in the active site critical for the foxglove P450_{scc}'s sterol cleavage ability. Identifying the foxglove P450_{scc} is a crucial step toward completely elucidating digoxin biosynthesis and expanding the therapeutic applications of digoxin analogs in future work.

Cardiac glycosides extracted from the foxglove plant *Digitalis lanata* have been used for treating congestive heart failure since 1785¹. Digoxin, a widely prescribed cardiac glycoside, is listed as an essential medicine by the World Health Organization². About 400,000 patients are prescribed digoxin in the United States, making it one of the most prescribed plant natural products³. Recent research has broadened the medicinal applications of cardiac glycosides for treating viral infection, inflammation, cancer, hypertension, and neurodegenerative diseases^{4–11}.

Due to the prominence of digoxin in medicine, the study of cardiac glycoside biosynthetic pathways dates back to the 1960s. Radiolabeling studies suggested cholesterol as the precursor for digoxin¹². While this is generally accepted, controversies remain since cholesterol is a minor sterol in plants. The exact biosynthetic pathway of digoxin remains enigmatic half a century after the initial work¹³. The hypothetical cardiac glycoside biosynthetic pathway starts with cholesterol, which undergoes nine enzyme-catalyzed steps to digoxigenin, the aglycone of digoxin¹³. Currently, the only known enzymes in the pathway are 3β -hydroxysteroid dehydrogenase (3β HSD) and

progesterone- 5β -reductase ($P5\beta R$ and $P5\beta R2$)^{14–16}. The first and rate-limiting enzyme, cytochrome P450 sterol side chain cleaving enzyme (P450_{scc}), along with all other enzymes, has not been identified yet^{13,17}. The foxglove P450_{scc} is thought to convert cholesterol to pregnenolone through a reaction identical to mammalian P450_{scc}, catalyzing the rate-limiting step in animal steroid hormone synthesis¹⁸. However, the plant P450_{scc} has not been isolated and characterized since its first description by Pilgrim in 1972¹⁹. Hence, the direct sterol precursor for digoxin biosynthesis remains ambiguous. Indirect evidence suggests that phytosterols, including campesterol, stigmasterol, and sitosterol, may also be precursors for digoxin^{12,19–23}.

In this study, we utilized a high-quality transcriptome of *D. lanata* to identify the foxglove P450_{scc}. Characterizing the foxglove P450_{scc} validated its sterol cleaving activity in tobacco and yeast. Investigating the foxglove P450_{scc} substrate preference uncovered the identity of sterol precursors for digoxin biosynthesis. Phylogenetic analysis suggests that this enzyme evolved from the *CYP87A* family. Protein modeling and mutagenesis revealed critical amino acids for foxglove P450_{scc}'s sterol-cleaving activity. The foxglove P450_{scc} is the first plant

¹Department of Biological Sciences, University at Buffalo, the State University of New York, Buffalo, NY, USA. ²These authors contributed equally: Emily Carroll, Baradwaj Ravi Gopal. ✉e-mail: zhenw@buffalo.edu

P450_{sc} identified and does not share substantial homology with the animal P450_{sc}.

Results

Transcriptome assembly and annotation

Total RNA from leaf and root tissues, including three biological replicates and two technical replicates from each tissue, were pooled to generate a reference transcriptome of *D. lanata*. We performed de novo assembly of the transcriptome from 173,448,870 Illumina raw reads with an average length of ~100 bp. The assembled transcriptome contains 317,983 transcripts with an N50 of 1712 bp (Table 1, Supplementary Fig. 1). The Benchmarking Universal Single-Copy Orthologs (BUSCO) score for the transcriptome was 94.6%, indicating that the transcriptome was near complete. A total of 190,755 transcripts at least 300-bp long were annotated using publicly available databases, including the NCBI non-redundant protein database (nr) and the UniProt database, each annotated 84.6% and 48.3% of the 190,755 transcripts, respectively^{24,25}. The transcripts were found to match best with genes of other Lamiales species, including *Sesamum indicum*, which covered 75.3% of the transcriptome (Supplementary Fig. 1). 113,221 non-redundant unigenes were categorized by gene ontology (GO) and Kyoto Encyclopedia of Genes and Genomes (KEGG) pathway classification^{26,27} (Supplementary Fig. 2). KEGG analysis revealed 5,683 unigenes in 412 KEGG pathways, among which were pathways for terpenoid and steroid biosynthesis (Supplementary Fig. 3). UniProt annotation identified 7517 transcription factors and regulators, 4226 protein kinases, and 22,549 simple sequence repeats (SSR) as genetic markers (Table 1, Supplementary Fig. 4, Supplementary Table 1). The annotated transcriptome presented here provides a comprehensive representation of transcripts in the root and leaf tissues of *D. lanata*.

Genes for sterol biosynthesis are differentially expressed

Since cardiac glycosides are only present in leaves but not roots (Fig. 1a), we asked if phytosterol and cholesterol biosynthetic genes are overexpressed in leaves. Indeed, genes encoding rate-limiting enzymes in phytosterol and cholesterol pathways were overexpressed in leaves (Fig. 1b). Squalene epoxidase (SQE), a rate-limiting step in sterol biosynthesis, showed higher relative transcript abundance in leaves²⁸. Sterol side-chain reductase (SSR1) is a known bottleneck enzyme²⁹ in cholesterol and phytosterol biosynthesis. Its transcript is also more abundant in *D. lanata* leaves. C4 sterol methyl oxidase 3 (SMO3), unique to the cholesterol pathway, is also more abundant in leaves. It catalyzes the rate-limiting step of 4-methyl elimination in the cholesterol pathway²³. Indeed, *D. lanata* leaves have higher cholesterol levels than roots, whereas the total sterols in these two tissues are comparable (Supplementary Fig. 5). Another gene with higher transcript abundance in leaves is the sterol C-14 reductase

(C14-R)³⁰, a shared enzyme between phytosterol and cholesterol pathways.

Analysis of the three known genes involved in digoxin biosynthesis shows that only *3βHSD*'s transcript was more abundant in leaves. While *P5βR*'s relative transcript abundance is the same in both tissues, *P5βR2*'s transcript is more abundant in roots. Since digoxin and sterols are triterpene derivatives, we also analyzed the differential relative transcript abundance of terpenoid biosynthetic genes (Supplementary Fig. 6). The methylerythritol phosphate (MEP) pathway for terpenoid synthesis and triterpene pathways are induced in leaves, agreeing with the compartmentalization of the MEP pathway in the chloroplast³¹.

Identifying two candidate genes as *D. lanata* P450_{sc}

The first step of the digoxin pathway is cleaving a sterol by a cytochrome P450_{sc} to generate pregnenolone¹³. Interpro scan identified 438 enzymes annotated as cytochrome P450s (CYPs) (Pfam: PF00067)^{32,33} from the transcriptome. CYPs from *Arabidopsis* and CYPs in *D. lanata* were used to construct a phylogenetic tree for CYP subfamily classification (Supplementary Fig. 7). Quantifying relative transcript abundance identified 104 CYP transcripts overexpressed in the leaves (Supplementary Fig. 8). Among these CYPs, only those members of subfamilies relevant to sterol/brassinosteroid biosynthesis were included for future analysis. Thirteen full-length CYP transcripts were identified as potential P450_{sc} (Fig. 2a). We focused on *DICYP87A4* and *DICYP90A1* because *DICYP87A4* was highly induced in leaves, and CYP90A1 is known to oxidize the 22(S)-hydroxycampesterol³⁴. qRT-PCR confirmed that *DICYP87A4* was expressed much higher in leaves compared to *DICYP90A1* (Fig. 2b). Therefore, these two transcripts were identified as P450_{sc} candidates and cloned from cDNA for functional validation by tobacco transient expression assay.

Tobacco expression identified *D. lanata* P450_{sc} as CYP87A4

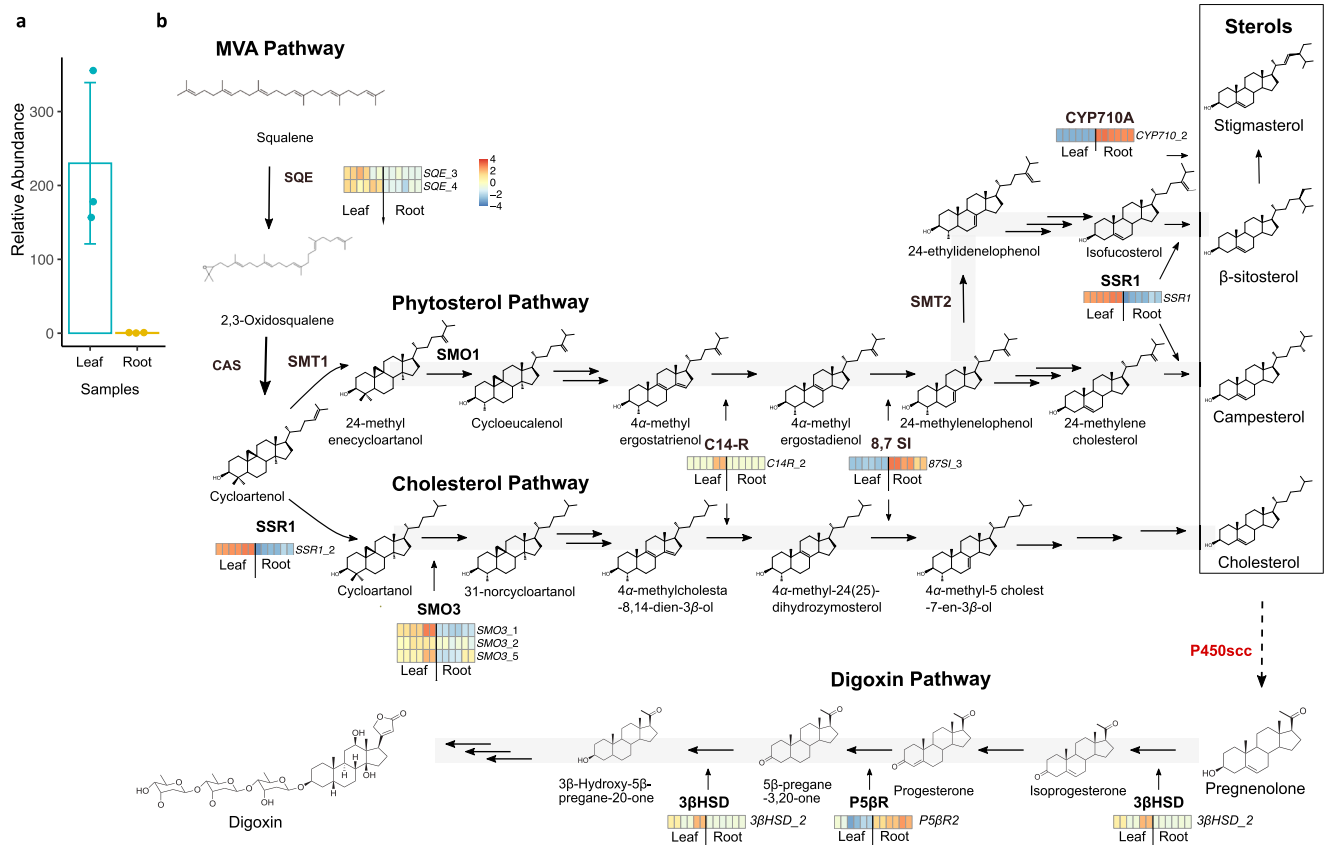
To test the two candidates, we employed the tobacco transient expression experiment. Tobacco does not produce digoxin but has sterol substrates for the P450_{sc}³⁵. Therefore, it is an ideal system for functionally characterizing the P450_{sc} enzyme. The two candidates, *DICYP87A4* and *DICYP90A1*, and the two known pathway enzymes, *3βHSD* and *P5βR*, were expressed in tobacco leaves (Fig. 2c, set 1). Following their expression, products of these enzymes, including progesterone (compound 2), 5β-pregnane-3,20-dione (compound 3), and 3β-hydroxy-5β-pregnane-20-one (compound 4), were detected (Fig. 2c, set 1, Supplementary Fig. 9). The direct product of P450_{sc}, pregnenolone (compound 1), was not seen in set 1 potentially due to its quick turnover through *3βHSD*. Note that the minor peak is not pregnenolone due to the different retention time compared to the pregnenolone standard. In fact, *D. lanata* leaves do not produce detectable amounts of pregnenolone but produce the downstream pathway intermediates (Supplementary Fig. 10). Omitting the *DICYP87A4* abolished the reactions (set 2), whereas taking out the *DICYP90A1* (set 3) had no effect. Expressing *DICYP87A4* alone resulted in the production of pregnenolone (set 4), whereas expressing *DICYP90A1* alone (set 5) did not produce pregnenolone. These data strongly support the hypothesis that *DICYP87A4* is the P450_{sc} of the digoxin pathway.

Determining the sterol substrates of CYP87A4

The tobacco expression system cannot determine the sterol substrate of *D. lanata* P450_{sc} because tobacco contains a mixture of cholesterol and phytosterols. Thus, we turned to the in vivo yeast expression since yeast does not produce cholesterol or phytosterols. However, feeding yeast with different sterols is challenging due to their hydrophobicity. Therefore, we used previously engineered yeast strains that produce various sterols, including cholesterol, campesterol, 7-dehydrocholesterol, and desmosterol (Fig. 3a, Supplementary Fig. 11)³⁵. We also included a wildtype yeast that produces ergosterol. When

Table 1 | Summary of Transcriptome data

Transcriptome assembly data	
Total no. of reads	173,448,870
No. of reads assembled	173,445,956
Transcripts	317,983
N50 value	1712 bp
Transcriptome Annotation Data	
Full-length transcripts	121,298
Transcripts annotated by UniProt	92,133
BUSCO	94.60%
Transcription factors and regulators	7517
Protein kinases	4226
simple sequence repeats (EST-SSR)	22,549



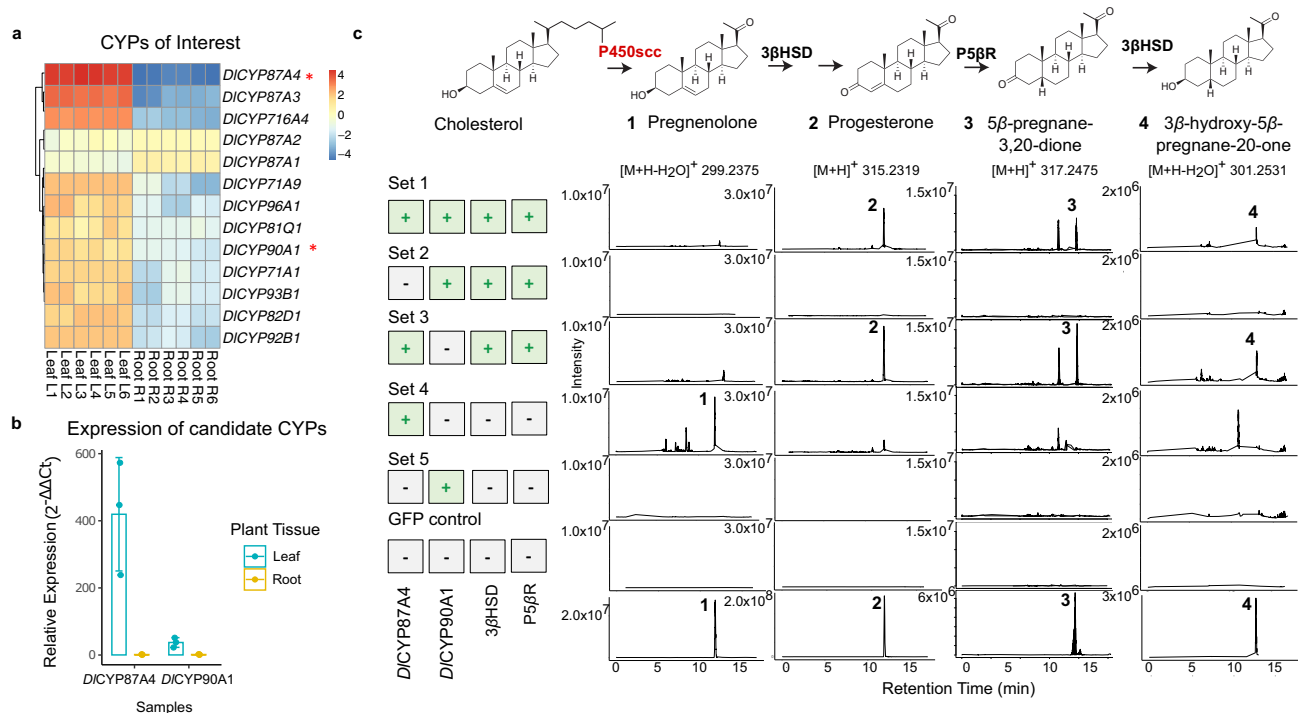


Fig. 2 | Identifying and characterizing candidate *D. lanata* P450_{scc}s in tobacco. **a** Quantifying the relative transcript abundance from candidate genes in root and leaf tissues of *D. lanata*. **b** qRT-PCR quantified relative transcript abundance of top candidate genes, *DICYP87A4* and *DICYP90A1*. Data represent the average ± SD of three biological replicates. **c** LC/MS data from tobacco leaves transiently expressing candidate genes in various combinations. The theoretical m/z values of parent ion adducts are given. Detected m/z values of peaks are within 5 ppm of the

theoretical value. Set 1 contained full-length *DICYP87A4*, *DICYP90A1*, *3βHSD*, and *P5βR*. Note the minor peak is not pregnenolone because of the different retention time compared to the pregnenolone standard. Set 2 contained *DICYP90A1*, *3βHSD*, and *P5βR*. Set 3 contained *DICYP87A4*, *3βHSD*, and *P5βR*. Set 4 contained *DICYP87A4* only. Set 5 contained *DICYP90A1* only. GFP control: negative control expressing a green fluorescent protein (GFP) in tobacco. The bottom panel shows the authentic standards of the four expected pathway intermediates.

DICYP87A4 and the putative *D. purpurea* P450_{scc} (*DpCYP87A*) but differ from the canonical CYP87As (Fig. 5c), suggesting that they are important for the sterol cleaving activity. Reverting A355 to leucine or L357 to alanine, as in the canonical *DICYP87A1*, abolished the campesterol side chain-cleaving activity, whereas the S123A mutation had no effect (Fig. 5d). A355 and L357 likely stabilize the steroid by forming hydrophobic interactions with the four steroid rings (Fig

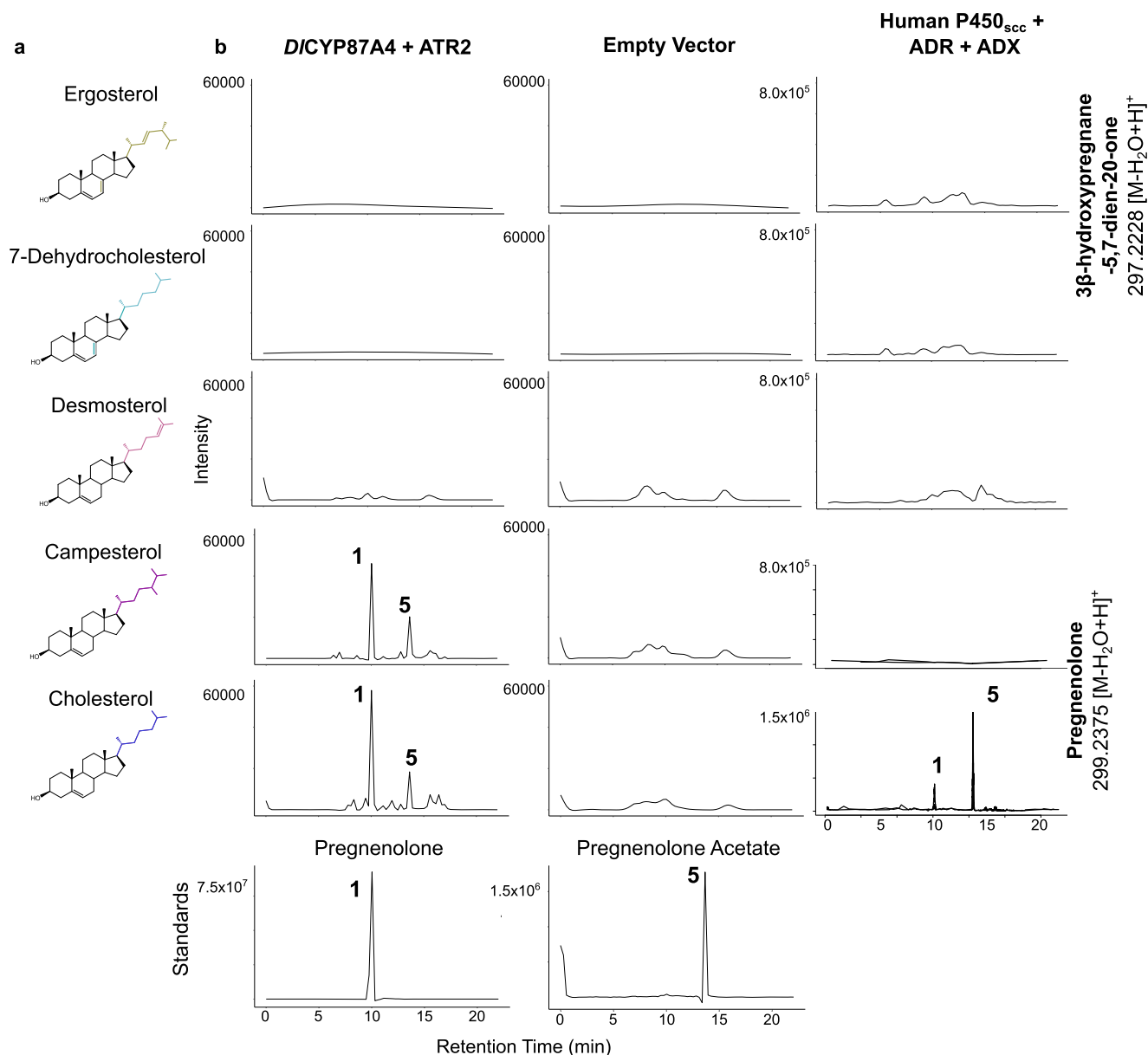


Fig. 3 | Characterizing the *D. lanata* CYP87A4 in *S. cerevisiae* strains producing various sterols. **a Sterols the yeast strains produce. **b** Extracted ion chromatograms from yeast expressing the full-length *DICYP87A4* and *ATR2* or the human *P450_{scc}* with its redox partners, adrenodoxin (*ADX*) and adrenodoxin reductase**

(*ADR*). The theoretical *m/z* values of parent ion adducts are given. Detected *m/z* values of peaks are within 5 ppm of the theoretical value. The bottom panel shows authentic standards of pregnenolone and pregnenolone acetate.

despite repetitive attempts, we do not rule out the possibility that these two mutations may also affect protein folding or stability. Comparing the substrate recognition sites of *DIP450_{scc}* and the human *P450_{scc}* revealed that the amino acids are distinct, although both sites are comprised mainly of non-polar amino acids, indicating hydrophobic interactions are the main driving force for substrate binding (Fig. 7). It remains unclear, however, if the stereochemistry of the 24-methyl group of campesterol affects the catalytic activity of *DIP450_{scc}*. Many plant species contain an epimeric mixture of 24(*R*)- and 24(*S*)-campesterol^{38–40}, the latter is called dihydrobrassicasterol. It is unclear if *D. lanata* contains both epimers or only the 24(*S*) stereoisomer.

The identification of *DIP450_{scc}* will enable the study of cardiac glycoside biosynthesis in other plant species, such as milkweed (*Asclepias*, *Calotropis*), wallflower (*Erysimum*), and oleander (*Nerium oleander*), to name a few⁴¹. Phylogenetic analysis showed that *Calotropis gigantea* might not have a duplicated CYP87A gene (Fig. 4),

assuming the publicly available *Calotropis* transcriptome is complete. Interestingly, the CYP87A is in the same phylogenetic clade as CYP90B1 that catalyzes the 22(*S*)-hydroxylation of campesterol, which is one of the three steps in the sterol side-chain cleaving reaction (Supplementary Fig. 7)¹⁸. It is likely that cytochrome P450s within this clan, including CYP708A, CYP88A, CYP702A, CYP85A, CYP90, CYP720A, and CYP724A, have the potential to evolve the sterol side-chain-cleaving activity. It remains unclear what is the function of the canonical CYP87A. It may oxidize a sterol or a triterpenoid since CYP87D16 from *Maesa lanceolata* oxidizes the C16 of β -amyrin⁴².

In conclusion, this work identified the rate-limiting and long-suspected *P450_{scc}* in *Digitalis* for the biosynthesis of digoxin. It is an essential step toward ultimately elucidating the digoxin biosynthetic pathway. This work will also open the door for biomanufacturing novel digoxin analogs with expanded medicinal value in microbial or plant systems.

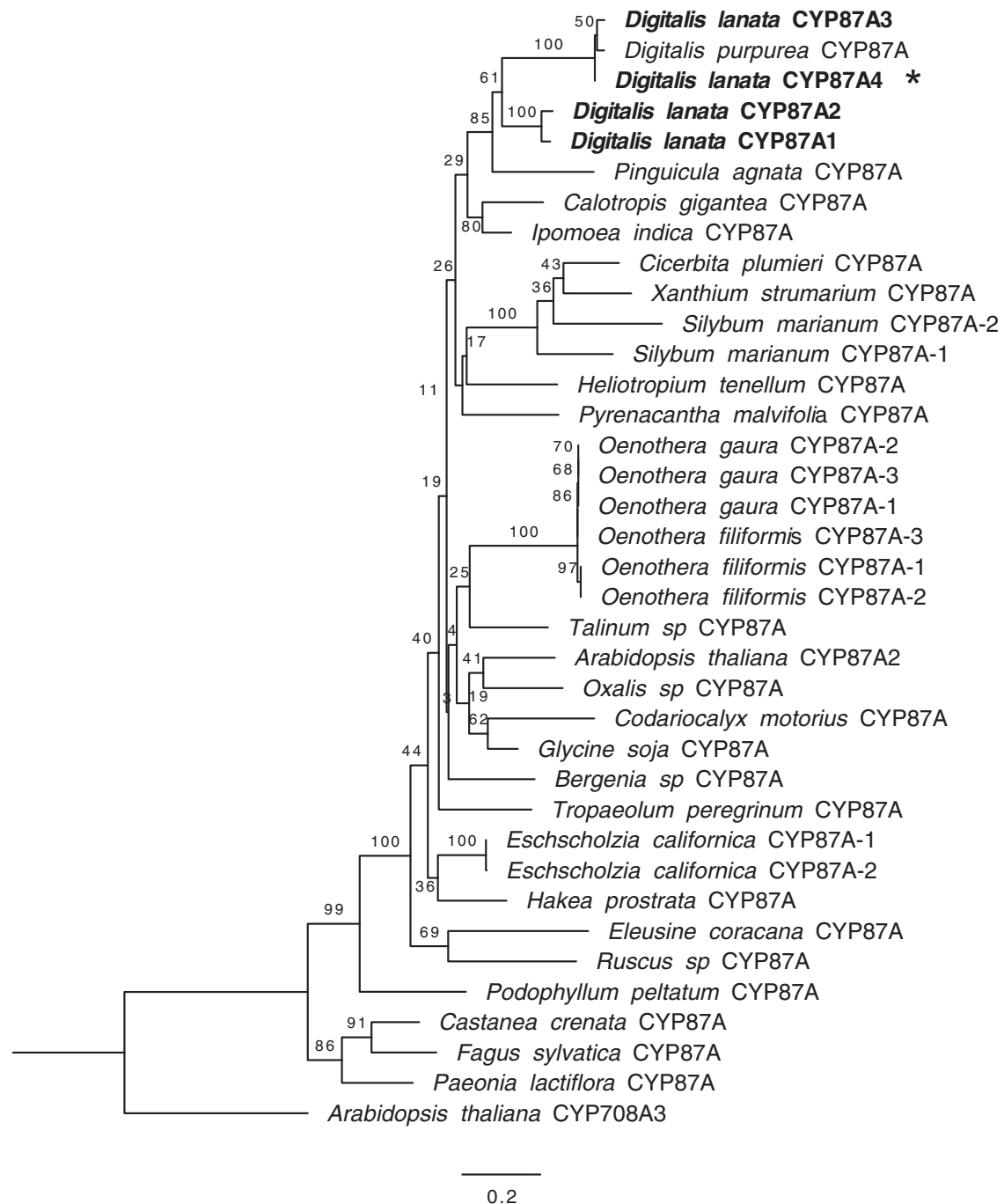


Fig. 4 | Maximum-likelihood phylogenetic tree of the CYP87A family members from eudicot plants. Protein sequences are retrieved from 1000 plant transcriptome project and are at least 50% identical to *DICYP87A4*. Bootstrap values

from 1000 replicates are shown at each node. *D. lanata* CYP87As are bolded. Asterisk denotes the characterized *DICYP87A4* in this study. The scale bar represents the mean number of substitutions per amino acid.

Methods

Plant material, RNA isolation, and sequencing

Digitalis lanata Ehrh seeds were procured from Strictly Medicinal (Williams, Oregon, USA). Seeds were germinated on the soil mix (57 g triple superphosphate, 85 g calcium hydroxide, 57 g bone meal, 369 g Osmocote (14-14-14), 99 g calcium carbonate, 25 L perlite, 50 L loosed peat and 25 L coarse vermiculite) and maintained in a growth chamber (Invitrogen, Clayton, Missouri, USA) under a light period of 16-h at 25 °C and a relative humidity of 60–80%.

Leaf and root tissues from three different seedlings were used to prepare the Illumina sequence library. Each seedling represents one biological replicate, and the total RNA from each replicate is split into

two technical replicates. Total RNA was isolated using the RNeasy Plant Mini Kit (Qiagen, Germantown, MD, USA). The sequencing library was prepared from total RNA using the TrueSeq Ribo-Zero Plant RNA library prep kit (Illumina, San Diego, CA, USA) that removes ribosomal RNA. A quality check of the library was carried out with an Agilent 2100 bioanalyzer. The library was sequenced using Illumina HiSeq 2500 to generate 100 bp paired-end raw reads.

Gene isolation and cloning

The detailed cloning method is included in the Supplementary Methods. Primers used are listed in Supplementary Table 3, and plasmid constructs are listed in Supplementary Table 4, respectively.

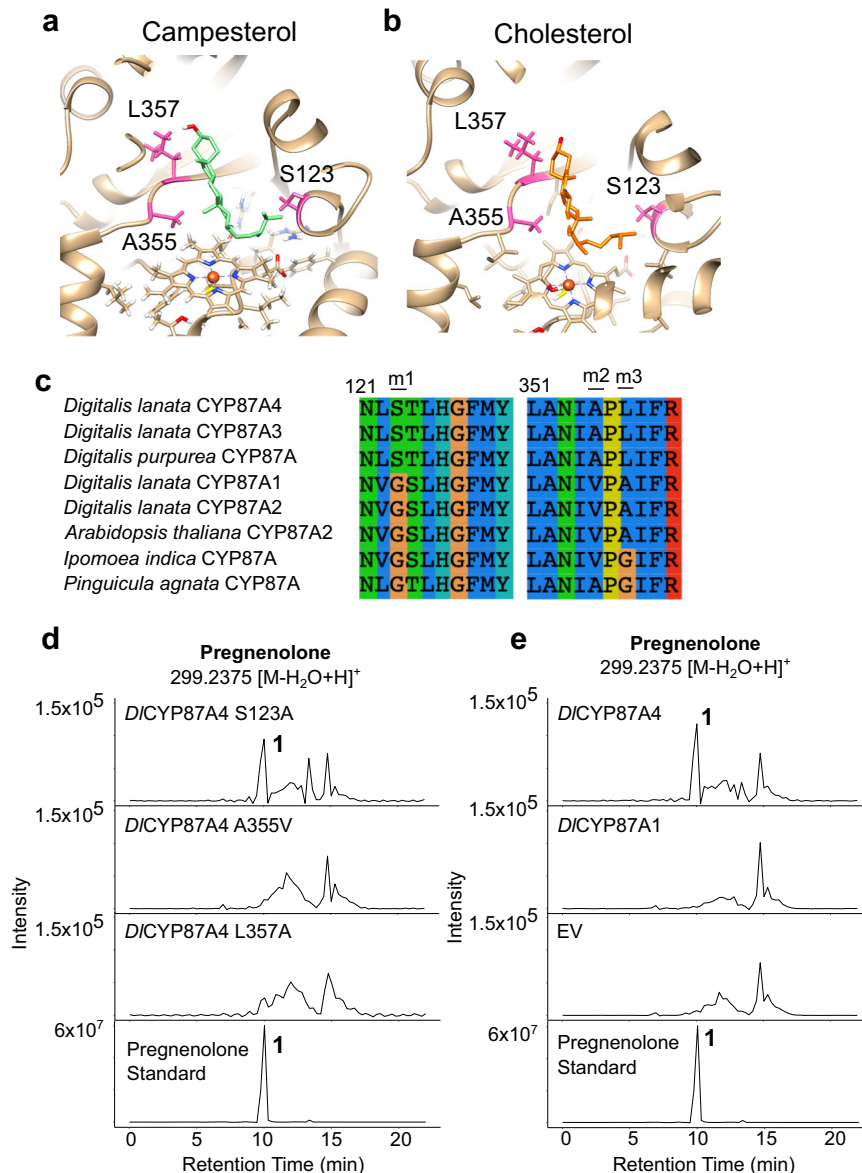


Fig. 5 | Protein modeling identified critical amino acids for *DICYP87A4*'s sterol cleaving activity. Docking of campesterol **a** and cholesterol **b** into the active site of the *DICYP87A4* protein model. Side chains of key amino acids S123, A355, and L357 are highlighted in pink. The protein model is truncated of a predicted N-terminal signal peptide of 31 amino acids. **c** Alignment of CYP87A subfamily enzymes to *D. lanata* and other CYP87A enzymes. Three locations that are different between *DICYP87A4* and the canonical *DICYP87A1* are indicated as follows; m1 (S123), m2

(A355), and m3 (L357). **d** Extracted ion chromatograms from campesterol-producing yeast expressing *DICYP87A4* mutants, including S123A, A355V, and L357A, along with ATR2. The theoretical m/z values of parent ion adducts are given. Detected m/z values of peaks are within 5 ppm of the theoretical value. **e** Campesterol-producing yeast expressing the wildtype *DICYP87A4* or the canonical *DICYP87A1* along with ATR2. Authentic standard for pregnenolone is shown in the bottom panel.

Tobacco transient expression

Agrobacterium transformation. pEAQ plasmids carrying genes of interest were transformed into the *Agrobacterium tumefaciens* strain AGL1 individually by the freeze-thaw method⁴³. The resulting strains were prepared for infiltration using a modified protocol as in Saxena et al.⁴⁴. Briefly, A single *Agrobacterium* colony containing one of the pEAQ plasmids was inoculated into 5 ml yeast extract broth (YEB) [5 g/L tryptone, 1 g/L yeast extract, 2.5 g/L Luria broth (Fisher Scientific, Waltham, MA, USA), 5 g/L sucrose, 0.49 g/L MgSO₄·7H₂O] with 50 mg/L kanamycin for pEAQ plasmid selection and 25 mg/L rifampicin for *A. tumefaciens* strain AGL1 selection. The bacterial cultures were grown 24 h at 28 °C with shaking at 220 rpm. Afterward, 0.5 ml of the seed culture was used to inoculate 25 ml of YEB with kanamycin (50 mg/L) and rifampicin (25 mg/L). The flasks were grown overnight at 28 °C, 220 rpm. The cultures were pelleted at 3000 g for 15 min, washed once

with 10 mL sterile double-distilled water (ddH₂O), and resuspended in MMA [10 mM MES (2-N-morpholinoethanesulfonic acid), pH 5.6, 10 mM MgCl₂, 100 μM acetosyringone]. The individually transformed strains were pooled together so that the final volume was 10 ml and each *A. tumefaciens* strain had a final OD₆₀₀ of 0.4. Then cultures were incubated for 2 to 4 h at 28 °C before infiltrating tobacco leaves.

Tobacco infiltration. The pooled *A. tumefaciens* was infiltrated into the underside of four- to six-week-old *Nicotiana benthamiana* new leaves using a needleless plastic syringe. The tobacco plants were grown in 16-h light and 8-h dark periods at 21 °C with a relative humidity of 60–80% and photon intensity of 120–150 μmol/m². Three leaves were infiltrated for each experimental set, and each set was completed on a single plant. As a negative control, *A. tumefaciens* transformed with pEAQ_GFP was infiltrated into a separate plant. Plants

were maintained in dark for 12 h to increase the agrobacterial infection and then shifted to light. The plants were maintained in normal conditions for four to six days. Once the fluorescence from GFP was intense when exposed to UV light, all infiltrated leaves were detached from the petiole, snap-frozen in liquid nitrogen, and ground into a fine powder. Metabolites were extracted with 1 ml 100% methanol (Fisher Scientific, Waltham, MA, USA) and heating at 65 °C for 10 min. They

were centrifuged at 17,000 g for 10 min, filtered through a 0.45 µm filter (VWR, Randor, PA, USA), and stored at -20 °C before LC/MS analysis.

Yeast *in vivo* expression assay

Sterol-producing yeasts were kindly provided from the Riezman lab (Supplementary Table 5)³⁵. Competent cells of these strains were prepared using the Frozen EZ Yeast Transformation II Kit™ (Zymo Research, Irvine, CA, USA). Starter cultures were grown in the SD-Leu medium at 30 °C overnight and then used to inoculate 25 mL SD-leu medium in triplicates in a shaking flask with an initial OD₆₀₀ of 0.2–0.4. Samples were harvested at 18 h and pelleted 3000 g for 5 min. Yeast cells were resuspended in 200 µL of TES buffer (50 mM Tris-HCl pH=7, 600 mM sorbitol, 10 g/L bovine serum albumin, 1.5 mM β-mercaptoethanol) and homogenized with an equal volume of 0.5 mm glass beads in a BBX24 Bullet Blender® homogenizer (Next Advance, Troy, NY, USA) at setting 8 at 4 °C for 4 min. A total of 300 µL of TES buffer was added to the lysed cells, and 400–500 µL of the yeast lysate was transferred into a capped glass tube, followed by adding 1 mL chloroform immediately. The sample was vortexed for 1 min, and the organic phase was transferred into a new glass test tube and dried under a stream of air. The sample was resuspended in 100 µL methanol, centrifuged at 17,000 g for 10 min, and the supernatant was transferred into a LC/MS vial and stored at -20 °C until use.

LC/MS analysis for pregnane intermediates in the digoxin pathway

Samples were analyzed using a LC/MS² instrument, a Thermo Scientific Q-Exactive Focus™, a hybrid quadrupole and orbitrap mass analyzer (Fisher Scientific, Waltham, MA, USA) and Thermo Scientific UltiMate 3000 UHPLC™ (Fisher Scientific, Waltham, MA, USA). A Waters XSelect CSH™ C18 HPLC column (SKU: 186005257, Waters, Milford, MA, USA) with a particle size of 3.5 µm, an internal diameter of 2.1 mm, and a length of 150 mm was used for separation. The column was set to 25 °C with the back pressure in the range of 130–150 psi. *Digitalis lanata* and tobacco extract samples in biological triplicates were analyzed as previously described^{45,46}. For analyzing pregnenolone and pregnenolone acetate from yeast samples, the following protocol was

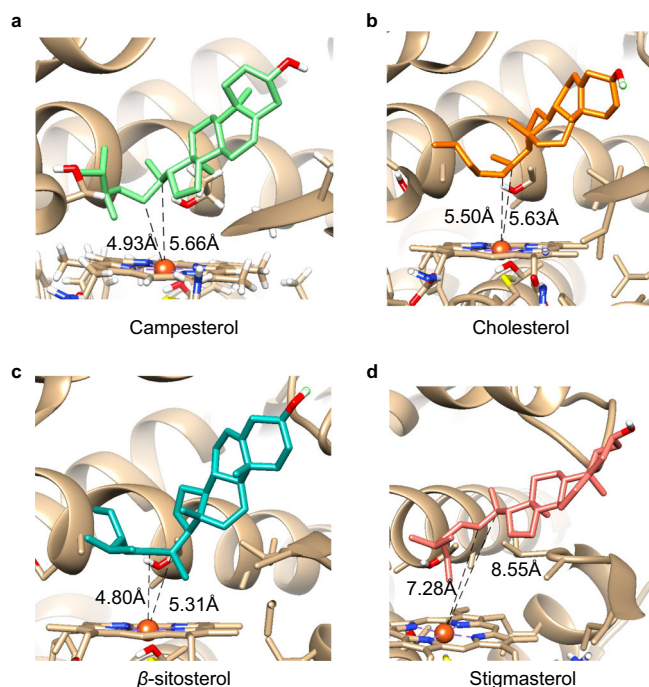


Fig. 6 | Docking cholesterol and phytosterols to the active center of the *D1P450_{sec}*. Docking simulations of *D1CPY87A4* with **a** campesterol, **b** cholesterol, **c** β-sitosterol, and **d** stigmasterol. Dashed lines show the distances of C20 and C22 to the heme center. Docking conformations shown are of the lowest energy in each simulation.

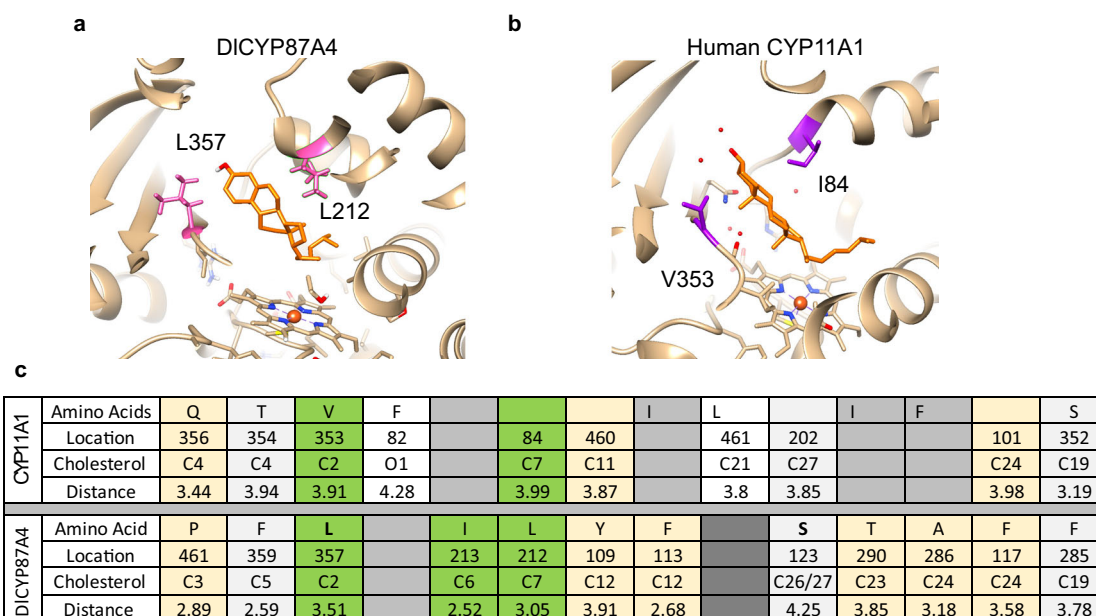


Fig. 7 | Substrate binding sites of the *D1P450_{sec}* and the human *P450_{sec}*. Comparison of substrate recognition sites of *Digitalis lanata* CYP87A4 **a** and human CYP11A1 **b**. Cholesterol is docked to the active sites. Amino acids at near-identical positions of *D1CYP87A4* and CYP11A1 are shown. **c** List of active-site amino acids

within 4.5 Å to cholesterol in *D1CYP87A4* and human CYP11A1. Green: similar amino acids in the two active sites; tan: hydrophobic amino acids in both active sites; gray: distinct amino acids.

developed. The mobile phase A was water with 0.1% formic acid and mobile phase B was acetonitrile with 0.1% formic acid, with a flow rate of 200 $\mu\text{L min}^{-1}$. Gradient started with 40% mobile phase B for 2 min followed by a linear gradient of 40% to 95% B from 2 to 11 min, held for 5 min, and brought back to initial conditions of 40% mobile phase B in 6 min. The sample injection volume was 20 μL , and the injection cycle time set to automatic with no sample splitting. The eluents were ionized by electron spray ionization (ESI) and analyzed in the positive ion mode. The full scan range is 100–1200 m/z at resolution of 70,000, inclusion error of ± 5 ppm and automatic gain control (AGC) of 1 million. The resolution for ddMS² is 17,500 with collision energies at 10, 30, and 60 eV, isolation window of 3.0 m/z , and AGC of 8000. The scan rate was set at automatic. The mass spectrometer was regularly calibrated to ensure mass accuracy. Qualitative analysis was performed using the XCalibur™ (v. 4.4.16.14) software. Raw files were converted to.mzML files using MSConvert (v. 3.0.21040), and chromatograms and spectra were generated in R (v. 4.2.0) using the XCMS (v. 3.18.0) and Spectra (v. 1.6.0) packages^{47,48}.

Phylogenetic analysis

Transcriptome sequences used for the CYP87A tree were retrieved by BLASTing the *DICPY87A4* transcript against the 1000 Plant Transcriptome (IKP) database using tBLASTx^{37,49} under default parameters. Sequences were filtered, and only those within 400–600 amino acids long and had a start codon were retained. *A. thaliana* CYP87A2 was used as a reference, and CYP708 was used as an outgroup.

All trees were constructed by aligning protein sequences using MAFFT⁵⁰. Aligned sequences were trimmed using trimAl⁵¹. The phylogenetic tree was constructed using RAXML-NG (v. 1.0.1) with the all-in-one Maximum likelihood (ML) tree search and slow bootstrapping with 1000 replicates⁵².

Protein modeling and docking

A protein model for the *D. lanata* P450_{sec} (*DICYP87A4*) was generated using Alphafold2 through the ColabFold platform v1.4^{53,54}. The MSA mode used was MMseqs2, and all other parameters were the default⁵⁵. Five models were generated, and model 3 was used for further analysis based on Predicted Aligned Error (PAE) and predicted local distance difference test (pLDDT) scores (Supplementary Fig. 15). Docking of sterols was performed using Chimera version 1.16 and Autodock Vina version 1.1.2^{56,57}.

Statistics

Total lanatoside quantification. The data are normalized by dry weight and represent the average \pm SD of three biological replicates.

Transcriptome heatmaps. Three biological replicates with two technical replicates each from roots and leaves were used to generate heatmaps. EdgeR was used to conduct the differential expression analysis to obtain log₂FPKM (transcript per million mapped reads). The significance cutoff for overexpression in leaf is $P < 0.05$.

qRT-PCR. Three biological replicates and two technical replicates were included for each sample. The mean of the two technical replicates' Ct values was normalized against that of the polyubiquitin 10 gene (*UBQ10*) to calculate the ΔCt . ΔCt value was then normalized against the mean ΔCt of roots to derive the $\Delta\Delta\text{Ct}$ value.

Reporting summary

Further information on research design is available in the Nature Portfolio Reporting Summary linked to this article.

Data availability

Data generated and analyzed are included in the published article and its supporting information files. *D. lanata* raw RNA-seq reads and the

assembled transcriptome are deposited into the Gene Expression Omnibus database (Accession: [GSE224014](https://doi.org/10.1038/s41467-023-39719-4)). LC/MS² and GC/MS data are available in the Metabolites database (Accession: [MTBLS7993](https://doi.org/10.1038/s41467-023-39719-4)). *D. lanata* CYP87A1-4 sequences are available in Supplementary Data 1, 2 and GenBank database (Accession: [OR134561](https://doi.org/10.1038/s41467-023-39719-4), [OR134562](https://doi.org/10.1038/s41467-023-39719-4), [OR134563](https://doi.org/10.1038/s41467-023-39719-4), [OR134564](https://doi.org/10.1038/s41467-023-39719-4)). Source data are provided with this paper.

References

1. Withering, W. *An account of the foxglove, and some of its medical uses.* (Swinney, 1785).
2. World Health Organization. WHO model list of essential medicines - 22nd list, 2021. *Tech. Doc.* (2021).
3. Medical Expenditure Panel Survey. Digoxin drug usage statistics, United States, 2013–2020. *ClinCalc DrugStats Database* (2022).
4. Mekhail, T. et al. Phase 1 trial of Anvirel™ in patients with refractory solid tumors. *Invest. N. Drugs* **24**, 423–427 (2006).
5. Srivastava, M. et al. Digitoxin mimics gene therapy with CFTR and suppresses hypersecretion of IL-8 from fibrosis lung epithelial cells. *Proc. Natl Acad. Sci. USA* **101**, 7693–7698 (2004).
6. Su, C.-T. et al. Anti-HSV activity of digitoxin and its possible mechanisms. *Antivir. Res.* **79**, 62–70 (2008).
7. Prassas, I. & Diamandis, E. P. Novel therapeutic applications of cardiac glycosides. *Nat. Rev. Drug Discov.* **7**, 926–935 (2008).
8. Piccioni, F., Roman, B. R., Fischbeck, K. H. & Taylor, J. P. A screen for drugs that protect against the cytotoxicity of polyglutamine-expanded androgen receptor. *Hum. Mol. Genet.* **13**, 437–446 (2004).
9. Kim, N. et al. Cardiac glycosides display selective efficacy for STK11 mutant lung cancer. *Sci. Rep.* **6**, 1–11 (2016).
10. Botelho, A. F. M., Pierezan, F., Soto-Blanco, B. & Melo, M. M. A review of cardiac glycosides: structure, toxicokinetics, clinical signs, diagnosis and antineoplastic potential. *Toxicol.* **158**, 63–68 (2019).
11. Ziff, O. J. & Kotecha, D. Digoxin: the good and the bad. *Trends Cardiovasc. Med.* **26**, 585–595 (2016).
12. Wickramasinghe, J. A. F., Hirsch, P. C., Munavalli, S. M. & Caspi, E. Biosynthesis of plant sterols. VII. The possible operation of several routes in the biosynthesis of cardenolides from cholesterol. *Biochemistry* **7**, 3248–3253 (1968).
13. Kreis, W. The foxgloves (*Digitalis*) revisited. *Planta Med.* **83**, 962–976 (2017).
14. Herl, V., Fischer, G., Müller-Uri, F. & Kreis, W. Molecular cloning and heterologous expression of progesterone 5 β -reductase from *Digitalis lanata* Ehrh. *Phytochemistry* **67**, 225–231 (2006).
15. Finsterbusch, A., Lindemann, P., Grimm, R., Eckerskorn, C. & Luckner, M. $\Delta 5$ -3 β -hydroxysteroid dehydrogenase from *Digitalis lanata* Ehrh. - A multifunctional enzyme in steroid metabolism? *Planta* **209**, 478–486 (1999).
16. Pérez-Bermúdez, P., Moya García, A. A., Tuñón, I. & Gavidia, I. *Digitalis purpurea* P5 β R2, encoding steroid 5 β -reductase, is a novel defense-related gene involved in cardenolide biosynthesis. *N. Phytol.* **185**, 687–700 (2010).
17. Lindemann, P. & Luckner, M. Biosynthesis of pregnane derivatives in somatic embryos of *Digitalis lanata*. *Phytochemistry* **46**, 507–513 (1997).
18. Strushkevich, N. et al. Structural basis for pregnenolone biosynthesis by the mitochondrial monooxygenase system. *Proc. Natl Acad. Sci. USA* **108**, 10139–10143 (2011).
19. Pilgrim, H. Cholesterol side-chain cleaving enzyme Aktivitat in keimlingen und in vitro kultivierten gewebe von *Digitalis purpurea*. *Phytochemistry* **11**, 1725–1728 (1972).
20. Kreis, W., Hensel, A. & Stuhlemmer, U. Cardenolide biosynthesis in foxglove. *Planta Med.* **64**, 491–499 (1998).
21. Aberhart, D. J., Lloyd-Jones, J. G. & Caspi, E. Biosynthesis of cardenolides in *Digitalis lanata*. *Phytochemistry* **9**, 1539–1543 (1970).

22. Milek, F., Reinhard, E. & Kreis, W. Influence of precursors and inhibitors of the sterol pathway on sterol and cardenolide metabolism in *Digitalis lanata* Ehrh. *Plant Physiol. Biochem.* **35**, 111–121 (1997).
23. Raghavan, I., Ravi Gopal, B., Carroll, E. & Wang, Z. Q. Cardenolide increase in foxglove after 2,1,3-benzothiadiazole treatment reveals a potential link between cardenolide and phytosterol biosynthesis. *Plant Cell Physiol.* (2022). **pcac144**.
24. Sayers, E. W. et al. Database resources of the National Center for Biotechnology Information. *Nucleic Acids Res.* **48**, D9–D16 (2020).
25. Bateman, A. et al. UniProt: the universal protein knowledgebase in 2021. *Nucleic Acids Res.* **49**, D480–D489 (2021).
26. Ashburner, M. et al. Gene ontology: tool for the unification of biology. The Gene Ontology Consortium. *Nat. Genet.* **25**, 25–29 (2000).
27. Kanehisa, M., Sato, Y., Kawashima, M., Furumichi, M. & Tanabe, M. KEGG as a reference resource for gene and protein annotation. *Nucleic Acids Res.* **44**, D457–D462 (2016).
28. Yoshioka, H. et al. A key mammalian cholesterol synthesis enzyme, squalene monooxygenase, is allosterically stabilized by its substrate. *Proc. Natl Acad. Sci. USA* **117**, 7150–7158 (2020).
29. Lange, I., Poirier, B. C., Herron, B. K. & Lange, B. M. Comprehensive assessment of transcriptional regulation facilitates metabolic engineering of isoprenoid accumulation in *Arabidopsis*. *Plant Physiol.* **169**, 1595–1606 (2015).
30. Schrick, K. et al. FACKEL is a sterol C-14 reductase required for organized cell division and expansion in *Arabidopsis* embryogenesis. *Genes Dev.* **14**, 1471–1484 (2000).
31. Banerjee, A. & Sharkey, T. D. Methylerythritol 4-phosphate (MEP) pathway metabolic regulation. *Nat. Prod. Rep.* **31**, 1043–1055 (2014).
32. Quevillon, E. et al. InterProScan: protein domains identifier. *Nucleic Acids Res.* **33**, 116–120 (2005).
33. Finn, R. D. et al. Pfam: the protein families database. *Nucleic Acids Res.* **42**, 222–230 (2014).
34. Ohnishi, T. et al. CYP90A1/CPD, a brassinosteroid biosynthetic cytochrome P450 of *Arabidopsis*, catalyzes C-3 oxidation. *J. Biol. Chem.* **287**, 31551–31560 (2012).
35. Souza, C. M. et al. A stable yeast strain efficiently producing cholesterol instead of ergosterol is functional for tryptophan uptake, but not weak organic acid resistance. *Metab. Eng.* **13**, 555–569 (2011).
36. Cauet, G., Degryse, E., Ledoux, C., Spagnoli, R. & Achstetter, T. Pregnenolone esterification in *Saccharomyces cerevisiae*. A potential detoxification mechanism. *Eur. J. Biochem.* **261**, 317–324 (1999).
37. Leebens-Mack, J. H. et al. One thousand plant transcriptomes and the phylogenomics of green plants. *Nature* **574**, 679–685 (2019).
38. Tsukagoshi, Y. et al. Ajuga Δ 24-sterol reductase catalyzes the direct reductive conversion of 24-methylenecholesterol to campesterol. *J. Biol. Chem.* **291**, 8189–8198 (2016).
39. Yamada, J. et al. 24-Methyl- and 24-ethyl- Δ 24(25)-cholesterols as immediate biosynthetic precursors of 24-alkylsterols in higher plants. *Tetrahedron* **53**, 877–884 (1997).
40. Mulheirn, L. J. Identification of C-24 alkylated steranes by P.M.R. spectroscopy. *Tetrahedron Lett.* **14**, 3175–3178 (1973).
41. Oerther, S. E. Plant poisonings: common plants that contain cardiac glycosides. *J. Emerg. Nurs.* **37**, 102–103 (2011).
42. Moses, T. et al. Unraveling the triterpenoid saponin biosynthesis of the African shrub *Maesa lanceolata*. *Mol. Plant* **8**, 122–135 (2015).
43. Wise, A. A., Liu, Z. & Binns, A. N. Three methods for the introduction of foreign DNA into Agrobacterium. *Methods Mol. Biol. (Clifton, N. J.)* **343**, 43–53 (2006).
44. Saxena, P., Thuenemann, E. C., Sainsbury, F. & Lomonosoff, G. P. Virus-derived vectors for the expression of multiple proteins in plants. *Methods Mol. Biol.* **1385**, 39–54 (2016).
45. Ravi, B. G., Guardian, M. G. E., Dickman, R. & Wang, Z. Q. High-resolution tandem mass spectrometry dataset reveals fragmentation patterns of cardiac glycosides in leaves of the foxglove plants. *Data Br.* **30**, 1–8 (2020).
46. Ravi, B. G., Grace, M., Dickman, R. & Wang, Z. Q. Profiling and structural analysis of cardenolides in two species of *Digitalis* using liquid chromatography coupled with high-resolution mass spectrometry. *J. Chromatogr. A* **1681**, 460903 (2020).
47. Smith, C. A., Want, E. J., O’Maille, G., Abagyan, R. & Siuzdak, G. XCMS: Processing mass spectrometry data for metabolite profiling using nonlinear peak alignment, matching, and identification. *Anal. Chem.* **78**, 779–787 (2006).
48. Rainer, J. et al. A modular and expandable ecosystem for metabolomics data annotation in R. *Metabolites* **12**, 173 (2022).
49. Carpenter, E. J. et al. Access to RNA-sequencing data from 1,173 plant species: The 1000 Plant transcriptomes initiative (1KP). *Giga-science* **8**, 1–7 (2019).
50. Katoh, K. & Standley, D. M. MAFFT multiple sequence alignment software version 7: improvements in performance and usability article fast track. *Mol. Biol. Evol.* **30**, 772–780 (2013).
51. Capella-Gutiérrez, S., Silla-Martínez, J. M. & Gabaldón, T. trimAl: a tool for automated alignment trimming in large-scale phylogenetic analyses. *Bioinformatics* **25**, 1972–1973 (2009).
52. Stamatakis, A. RAxML version 8: a tool for phylogenetic analysis and post-analysis of large phylogenies. *Bioinformatics* **30**, 1312–1313 (2014).
53. Jumper, J. et al. Highly accurate protein structure prediction with AlphaFold. *Nature* **596**, 583–589 (2021).
54. Mirdita, M. et al. ColabFold: making protein folding accessible to all. *Nat. Methods* **19**, 679–682 (2022).
55. Steinegger, M. & Söding, J. MMseqs2 enables sensitive protein sequence searching for the analysis of massive data sets. *Nat. Biotechnol.* **35**, 1026–1028 (2017).
56. Tettersten, E. et al. UCSF Chimera—a visualization system for exploratory research and analysis. *J. Comput. Chem.* **13**, 1605–1612 (2004).
57. Trott, O. & Olson, A. J. AutoDock Vina: Improving the speed and accuracy of docking with a new scoring function, efficient optimization, and multithreading. *J. Comput. Chem.* **31**, 455–461 (2010).

Acknowledgements

We thank Dr. Howard Riezman at the University of Geneva for providing the sterol-producing yeast strains, Rian Hammond for providing plasmids encoding the human P450_{SCC}, Dr. George Lomonosoff at the John Innes Center and Leaf Systems for supplying the pEAQ vector, Dr. Valerie Freichs for assistance with chromatography work, and Dr. Donald Yergeau for RNA-seq at University at Buffalo. This project was supported by the Research Foundation for the State University of New York [71272] to Z. Q. Wang and the National Science Foundation [CHE-1919594] to the University at Buffalo Chemistry Instrument Center.

Author contributions

E.C., B.R.G., and Z.Q.W. designed research; E.C., B.R.G., I.R. and M.M. carried out experiments; E.C., B.R.G., I.R., M.M. and Z.Q.W. analyzed data; E.C., B.R.G., I.R. and Z.Q.W. wrote the paper.

Competing interests

The authors declare no competing interests.

Additional information

Supplementary information The online version contains supplementary material available at <https://doi.org/10.1038/s41467-023-39719-4>.

Correspondence and requests for materials should be addressed to Zhen Q. Wang.

Peer review information *Nature Communications* thanks Reuben Peters, Yong Wang and the other, anonymous, reviewer(s) for their contribution to the peer review of this work. A peer review file is available.

Reprints and permissions information is available at <http://www.nature.com/reprints>

Publisher's note Springer Nature remains neutral with regard to jurisdictional claims in published maps and institutional affiliations.

Open Access This article is licensed under a Creative Commons Attribution 4.0 International License, which permits use, sharing, adaptation, distribution and reproduction in any medium or format, as long as you give appropriate credit to the original author(s) and the source, provide a link to the Creative Commons license, and indicate if changes were made. The images or other third party material in this article are included in the article's Creative Commons license, unless indicated otherwise in a credit line to the material. If material is not included in the article's Creative Commons license and your intended use is not permitted by statutory regulation or exceeds the permitted use, you will need to obtain permission directly from the copyright holder. To view a copy of this license, visit <http://creativecommons.org/licenses/by/4.0/>.

© The Author(s) 2023